

See discussions, stats, and author profiles for this publication at: <https://www.researchgate.net/publication/332856058>

# Electrochemical Impedance Spectroscopy as a Performance Indicator of Water Dissociation in Bipolar Membranes

Preprint · May 2019

DOI: 10.26434/chemrxiv.8068238

CITATIONS

0

READS

129

5 authors, including:



**Boaz Izelaar**

Delft University of Technology

2 PUBLICATIONS 0 CITATIONS

[SEE PROFILE](#)



**Wilson A Smith**

Delft University of Technology

108 PUBLICATIONS 2,331 CITATIONS

[SEE PROFILE](#)

Some of the authors of this publication are also working on these related projects:



System-based Approaches for the Enhancement of Catalytic CO<sub>2</sub> Reduction Reactions [View project](#)



Rational design of carbon dioxide electroreduction catalysts using multiscale modeling [View project](#)

Cite this: *J. Mater. Chem. A*, 2019, 7, 19060

# Electrochemical impedance spectroscopy as a performance indicator of water dissociation in bipolar membranes†

Marijn A. Blommaert,<sup>a</sup> David A. Vermaas,<sup>ab</sup> Boaz Izelaar,<sup>a</sup> Ben in 't Veen<sup>c</sup> and Wilson A. Smith<sup>\*a</sup>

A bipolar membrane (BPM) can be used to maintain a pH difference in an electrolysis cell, which provides freedom to independently optimize the environments and catalysts used for paired redox reactions. A BPM consists of two physical layers, of which one is selective for the exchange of cations and the other for anions. The water dissociation reaction (WDR) splits water into protons and hydroxide ions under an electric field that concentrates at the interface of the two membrane layers. However, salt ions in commonly used electrolytes influence this WDR when they are present at the interface. Using electrochemical impedance spectroscopy (EIS), we observed the rate of water dissociation decrease in the presence of salt ions while also observing the diffusion and migration of these salt ions, showing a clear link between the peaks observed in EIS and ion crossover. In addition, we show how EIS can be used to *in situ* monitor the stability and ageing of a BPM, revealing that degradation of the BPM is more prominent in extreme pH electrolyte pairs compared to non-extreme electrolyte pairs. The *in situ* monitoring of the WDR and stability of a BPM are vital methods for adequate and consistent comparison of novel designs of BPM-based systems, where EIS allows for discriminating BPM characteristics from other components even during operation.

Received 2nd May 2019  
Accepted 12th July 2019

DOI: 10.1039/c9ta04592a

rsc.li/materials-a

## Introduction

The increasing concentration of greenhouse gases such as CO<sub>2</sub> in our atmosphere has destabilized Earth's climate, as confirmed by the most recent report from the Intergovernmental Panel on Climate Change (IPCC).<sup>1</sup> The consequences of a 1 °C increase of the global mean temperature compared to pre-industrial levels are already evident, requiring immediate actions to reduce our global CO<sub>2</sub> emissions and mitigate further dire consequences. With rapidly decreasing prices of renewable energy and an increasing electrification of the energy sector, a promising approach to close the carbon cycle with the production of valuable products is needed. This can be achieved by synthesizing chemicals and fuels using renewable energy *via* water electrolysis or the electrocatalytic reduction of carbon dioxide (CO<sub>2</sub>ER).

When considering either of these electrochemical routes at an industrially relevant scale, it is important to have a system

run at a high energy efficiency. In other words, the applied potential should be as close as possible to the thermo-neutral cell potential for the combined oxidation and reduction reactions. The importance of high energy efficiency arises from the relatively high contribution of electricity costs in electrochemical systems,<sup>2</sup> which makes achieving a high efficiency a necessity to compete with current chemical production means, where nearly all the fuels and commodity chemicals originate from fossil-based resources. However, the state-of-the-art electrolysis of water or CO<sub>2</sub> still has a low energy efficiency at high current densities due to large overpotentials for the relevant reduction–oxidation reactions, ohmic losses across the electrolyte and potential drops across an ion exchange membrane that separates the anode and cathode compartments.<sup>3–5</sup> Making matters more difficult, catalysts for the reduction and oxidation reactions perform better—*i.e.*, have a higher stability and lower overpotential—in different electrolytes with different pHs, thereby making a total system difficult to optimize with a single electrolyte.<sup>6,7</sup>

To integrate different electrolytes into a single electrochemical cell, a bipolar membrane (BPM) can be implemented. Recently, several studies have successfully observed stable operation and lower cell potentials using independent electrolyte pairs for water oxidation coupled to water reduction or CO<sub>2</sub>ER using a BPM.<sup>7–10</sup> A BPM consists of two physical layers, one which is selective for the exchange of cations (cation

<sup>a</sup>Department of Chemical Engineering, Delft University of Technology, 2629 HZ Delft, The Netherlands. E-mail: w.smith@tudelft.nl

<sup>b</sup>AquaBattery B.V., Lijnbaan 3C, Leiderdorp, 2352CK, The Netherlands

<sup>c</sup>Shell Global Solutions International B.V., Grasweg 31, 1031 HW Amsterdam, The Netherlands

† Electronic supplementary information (ESI) available. See DOI: 10.1039/c9ta04592a

exchange layer, CEL) and the other for anions (anion exchange layer, AEL). Under an applied potential or pH gradient across the BPM, the interface between these layers enhances the dissociation of water into protons and hydroxide ions, described by the water dissociation reaction (WDR).<sup>11–13</sup> At this membrane–membrane interface, a catalyst can be deposited to further improve the kinetics of the WDR. A great deal of research on understanding and improving the characteristics of a BPM focuses on the interface between the anion–cation exchange layers.<sup>14–16</sup>

The ion-exclusivity of a BPM, with two different layers and their fixed charges, should in theory be impermeable for any charged species transported through both layers. Since the ion-exclusivity is imposed by finite fixed charges of the membrane layers, a (limited) co-ion exchange will occur between the two different solutions. In monopolar membranes, co-ions are described as ions with the same charge as the fixed charges in the membrane layer. However, for the BPM, co-ions have a more ambiguous definition because of the different polarity in the two membrane layers. Here, we define co-ions as ionic salt species that do not participate in the WDR, *i.e.*, all ions except for  $H^+$  and  $OH^-$ . It is important to note that a CEL and an AEL in contact with electrolytes with very high or very low pH such as KOH and  $H_2SO_4$ , respectively, theoretically do not contain co-ions in the membrane layers. The contribution to the ionic current, equal to the electrical current through the cell, of each individual ion species is described by the transport number.<sup>17</sup> As this ionic current in the BPM is composed of a movement of co-ions and charge transport due to water dissociation, migration of co-ions lowers the efficiency of the water dissociation reaction<sup>18</sup> and thus negatively affects the overall cell efficiency.

Recent studies have shown the dependency of electrolyte pH and composition surrounding the BPM on the voltage response across the BPM in the presence of an applied current.<sup>13</sup> Depending on the electrolytes used, the  $i$ - $V$  curve typically contains a sharp increase of the voltage at a certain current density. After this initial increase, a plateau at a relatively constant current density,  $j_{\text{plateau}}$ , is observed until reaching the membrane voltage of water dissociation (0.829 V), where the current increases sharply with applied potential (see Fig. 1). However, in contrast to monopolar membranes, which also show activity towards the WDR above a limiting current density,<sup>19</sup> bipolar membranes have shown that charge transport can be dominated by the WDR below the plateau current density under certain conditions.<sup>20</sup> At higher current densities, the water dissociation efficiency increases further.<sup>12,18,21,22</sup> It is necessary to probe the electrochemical behavior of the interfacial layer to better understand the conditions that determine the WDR, and the relation with the  $i$ - $V$  curve and the plateau region.

One way to probe the WDR is *via* electrochemical impedance spectroscopy (EIS), which differentiates the various components of the BPM as electrical features that can be derived from impedance responses upon a varying frequency.<sup>17</sup> In this way, factors such as the finite conductivity of the membrane layers and electrolyte solutions are measured as an ohmic resistor, the diffusion boundary layer is shown as a constant phase element, and the sudden changes in charge density at the BPM interfaces

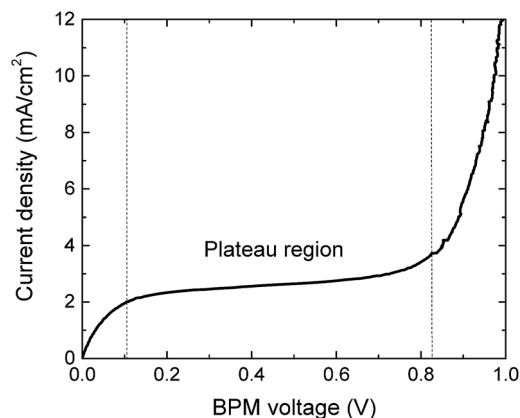


Fig. 1 Typical  $i$ - $V$  curve of a bipolar membrane in a salt electrolyte, with the plateau region between a BPM voltage of 0.1 to 0.8 V. A galvanodynamic scan was applied at a scan rate  $-0.01 \text{ mA cm}^{-2} \text{ s}^{-1}$  with 5 M NaCl in both compartments.

are shown as electrical double layers.<sup>23–28</sup> In this work, EIS is used to examine the equivalent circuit elements that represent a BPM separating two different pairs of electrolytes at various current densities, as schematically shown in Fig. 2. The results show that EIS is a useful tool to monitor ion transport in BPMs, which is composed of products of the WDR and crossover of co-ions through the BPM. Furthermore, a decrease of impedance features linked to decreased co-ion transport through the BPM was observed when the current exceeded  $j_{\text{plateau}}$ . These findings are important to understand the role of co-ions in supporting and inhibiting the WDR at currents below the plateau current density. In addition, EIS was able to monitor the stability of the BPM and its individual components during operation in an

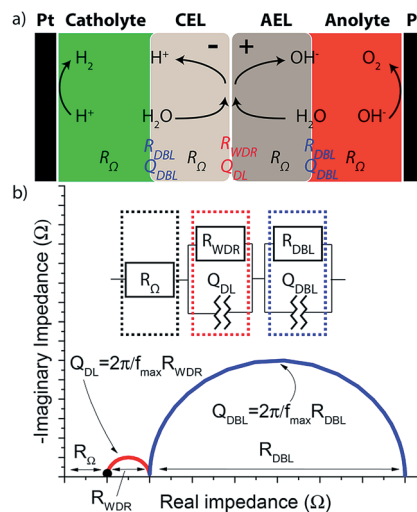


Fig. 2 (a) Schematic representation of individual components of the impedance response of a BPM in an electrochemical cell, with (black) ohmic losses of membrane and solution, (red) membrane–membrane interface where WDR occurs, and (blue) diffusion boundary region with a constant phase element. (b) The equivalent circuit used to describe the impedance results is shown with the corresponding Nyquist plot.

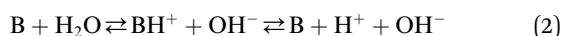
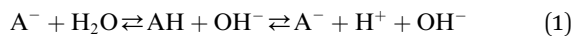
electrochemical cell by performing EIS before and after galvanostatic experiments. These experiments showed a degradation in the membrane layers as well as the WDR performance for a case with a pH difference of 14, but relatively stable conditions for a case with less extreme electrolytes.

## Theory

### Water dissociation reaction

A bipolar membrane has three electrochemical interfaces: two membrane–solution interfaces (CEL/catholyte and AEL/anolyte) and one internal interface (CEL/AEL). The latter is the membrane–membrane interface where the water dissociation reaction occurs when a reverse bias is applied to the system, with the negatively charged layer opposing the negative charged cathode.

The reaction rate of the WDR is  $5 \times 10^7$  times faster in a BPM than in aqueous electrolyte, which is enhanced by the electrochemical properties of a BPM.<sup>14</sup> There are multiple theories describing the WDR:<sup>14</sup> some focus on the Donnan equilibrium,<sup>29</sup> some on the second Wien effect,<sup>30</sup> and others on proton transfer reactions with fixed charges.<sup>31,32</sup> In the latter theory, which has the most realistic simulated reaction rates, weak acids and bases catalyze the WDR, shown in the following reaction schemes:



here AH and B are a weak acid and base, respectively. Both membrane layers perform one reaction dominantly, *e.g.* the cation exchange layer with negatively charged species would preferentially perform reaction (1), while the anion exchange layer with positively charged species preferentially performs reaction (2). To avoid the reverse reaction, separation of both  $H^+$  and  $OH^-$  *via* membrane charges with opposite charge is required, which implies that the WDR is most effective near the CEL/AEL interface.<sup>33</sup> A catalyst present at the interface between the AEL and CEL improves the kinetics of these reactions as well by lowering the activation energy—in this case, the reaction of (1) or (2), producing protons and hydroxide ions.<sup>14</sup>

### Electrochemical impedance spectroscopy

Electrochemical impedance spectroscopy can be used to examine the electronic responses of individual components of a membrane by varying the applied frequency.<sup>17</sup> An introduction of the theory behind the EIS data and interpretations is provided in the ESI.† Fig. 2(b) shows the proposed equivalent circuit describing the three components of a BPM. The first component is  $R_\Omega$ , related to the conductivity of the combined membrane layers. This component follows Ohm's law ( $V = IR$ ), and since there is no capacitive effect in  $R_\Omega$ , it is independent of frequency. The resistance can be determined from a Nyquist plot by measuring the distance between the origin and the start of the first semicircle. This value also includes the ohmic losses

of the electrolytes from the membrane to the reference electrodes.

The second component of the equivalent circuit describes the WDR, and the kinetics of this reaction are in the form of a resistance ( $R_{WDR}$ ). In parallel with the resistor is the electric double layer of the internal interface, represented as a non-ideal capacitor ( $Q_{DL}$ ). This  $RQ$ -network shows the typical semicircle of a charge transfer reaction,<sup>17</sup> in this case to produce protons and hydroxide ions.  $R_{WDR}$  is equal to the width of the semicircle, and  $Q_{DL}$  is the inverse of the angular velocity ( $\omega = 2\pi f$ ) of the peak height and  $R_{WDR}$ . Since a BPM typically has a non-uniform current distribution, the system cannot be described with an ideal capacitor. Instead, a constant phase element is used, including a non-ideality factor  $n$ , lying between 0 and 1, with  $n = 0$  being a resistor and  $n = 1$  an ideal capacitor.<sup>23</sup> Hurwitz and Dibiani (2003) described the water dissociation component of their equivalent circuit in combination with a component related to the proton gradient near the membrane–membrane interface.<sup>27</sup> However, in our and their experiments, there is no indication that this gradient component is required for successful fitting of the results, and it is therefore considered to be a part of the water dissociation component.

The third component relates to the diffusion boundary layer between the membrane layers and electrolytes. When ions are transported out of the membrane layer and surrounded by mobile charges with the same charge, they enter an electro-neutral solution with which they differ in concentration. This effect happens due to the Donnan exclusion in the membrane layer, which is the source of the Donnan potential between the diffusion layer of the electrolyte solution and the membrane layer.<sup>34,35</sup> This is especially true when the concentration of the protons or hydroxide ions is low in the electrolyte (*e.g.* in a bicarbonate electrolyte). Similar to the second component, the resistance that the transported ions encounter ( $R_{DBL}$ ) is in parallel with a non-ideal capacitor, represented by a constant phase element ( $Q_{DBL}$ ). These two elements both show non-linear behavior upon a variation of current. First, the resistance is created by concentration polarization at the membrane–electrolyte interface. Since impedance is the ratio of the voltage, which is described by the Donnan potential  $\Delta\Phi_{Donnan} = \ln(C_i/\bar{C}_i)$  with  $\bar{C}_i$  the concentration of species  $i$  in the membrane and the current, the resistance is non-linear dependent upon a varying current. This is because of the logarithmic behavior as well as the non-linear behavior of  $C_i/\bar{C}_i$  in non-steady state.<sup>36</sup> Second, the non-ideal capacitor, which is created by the change in charges at these interfaces, is also a function of concentration. Since the change in charge of all species in this region is not linear, the DBL is not linear,<sup>37</sup> as shown in Fig. 3 which gives a schematic representation of the concentration profile of three electrolytes of the membrane–solution interface. For example, for a CEL the concentration of the cations is equal to the sum of the concentrations of the fixed charges and the anions, which are present due to non-ideality of the membrane layer. Once a current is applied, cations migrate out of the CEL towards the cathode, and protons replenish the membrane layer to maintain electroneutrality. This is visible when  $KHCO_3$  is used as catholyte (left in Fig. 3). Due to the

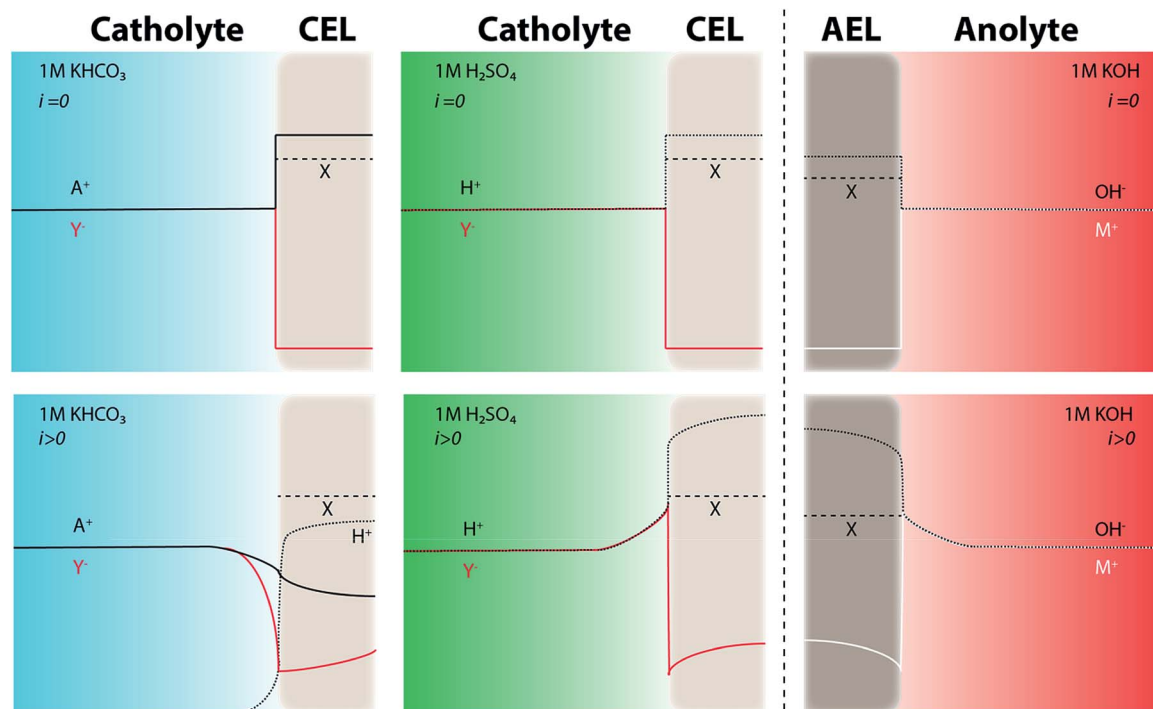


Fig. 3 Concentration profiles of electrolytes near ion exchange layer, in the diffusion boundary layer. Assuming that no ion exchange occurs when no current is applied, there is no DBL when  $i = 0$ . If  $i > 0$ , migration component results in an increased concentrations of present ions. At the membrane–solution interface, there is the double layer where no electroneutrality occurs, with  $X$  concentration of fixed charges,  $A^+$  and  $M^+$  concentration of cations and  $Y^-$  concentration of anions.

different diffusion coefficients in the membrane layer and electrolyte, a diffusion boundary layer is formed once a current is applied, which is dominated by the main carrier of the current, e.g.  $\text{OH}^-$  in the case of the AEL.

Most literature has focused on the first two components, since the third component is typically found at lower frequencies (<1 Hz) and requires a stable setup to perform long term measurements to reduce noise.<sup>24,25,27</sup> In addition to the experimental data present in the literature, also modelling has been performed of the electrochemical impedance response by Alcaraz *et al.* based on the Nernst–Planck and Poisson equations, describing the membrane–membrane interface as a p-n-junction.<sup>38</sup> The model does not include the diffusion boundary layers at the electrolyte–membrane interface, which is a limitation for comparing the results with this work. Yan *et al.* studied a BPM at lower frequency in their ESI; however, they described the third component as a Gerischer impedance coupling the diffusion boundary layer to a chemical reaction.<sup>39</sup> In our work, the EIS results from two different electrolyte pairs across a BPM are shown, indicating that the co-ion plays a role in the diffusion boundary layer as well as in the WDR component of the equivalent circuit.

## Methods

In this work, we compare two different electrolyte combinations across a BPM during electrolysis to determine the effect of co-ions on the water dissociation reaction. One electrolyte pair

theoretically contains no co-ions in the membrane layer ( $\text{H}_2\text{SO}_4$  as the catholyte and  $\text{KOH}$  as the anolyte), because  $\text{SO}_4^{2-}$  and  $\text{K}^+$  will be excluded from the CEL and AEL, respectively, based on ion-selectivity of the membrane layers. For simplicity, this case will be designated as the ‘no co-ions<sub>mem</sub>’ case, where the ‘mem’ indicates that this is only the case in ideal membrane layers. Another electrolyte pair,  $\text{KHCO}_3$  and  $\text{KOH}$ , does contain a co-ion in the CEL in the form of  $\text{K}^+$ , and is designated as the ‘co-ions’ case. Bicarbonate is often used as an electrolyte for the  $\text{CO}_2$  reduction reaction due to its buffer capacities and optimal pH to partially suppress the hydrogen evolution reaction.<sup>40</sup> Therefore this electrolyte was chosen to assess its compatibility with a BPM for use in a  $\text{CO}_2$ ER system. Specifications of the chemicals and materials used are described in the ESI.†

A commercially available Fumatech BPM was used in all experiments, which were performed with a SOLARTRON potentiostat (EnergyLab XM) in galvanostatic mode and three cycles of frequency to reduce noise. The frequency was varied from 10 kHz to 1 mHz. Bode plots shown here are smoothed with a Lowess method. EIS measurements were performed in a 4-electrode setup (Fig. 4) with two Ag/AgCl reference electrodes placed on both sides of the BPM, and the effective distance is therefore approximately 0.5 mm from the bipolar membrane in an aqueous H-cell configuration. The membrane has a surface area of 1.33  $\text{cm}^2$ . Working and counter electrodes are made of Pt-wires and each have a surface area of 2.83  $\text{cm}^2$ . Ageing experiments were performed in a flow cell (see Fig. S2†), with a membrane and electrode surface area of 10  $\text{cm}^2$ . Analysis

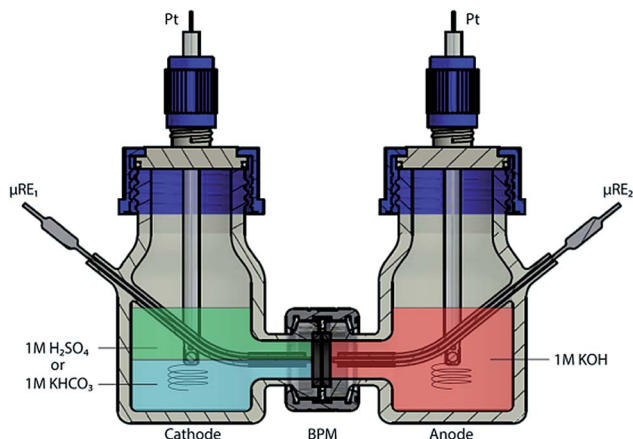


Fig. 4 Schematic illustration of impedance setup in H-cell configuration with the two used electrolytes ( $\text{H}_2\text{SO}_4$  and  $\text{KHCO}_3$ ) in the catholyte, separated from the anolyte (KOH) by a BPM.

of the impedance data was performed with ZView 2 (Scribner), and the fitting was performed with the equivalent circuit shown in Fig. 2, which will be used to indicate the performance of the individual components of the BPM discussed in the results.

## Results & discussion

Nyquist plots for the case of co-ions ( $\text{KHCO}_3$  vs. KOH) were obtained as a function of current density, shown in Fig. 5(a). As the current density increased, the diameter of the semicircle decreased, showing a lower resistance across the membrane. The variation of the origin of the semicircle is due to the changing of the position of the reference electrode in each experiment, and does not affect the resistive features associated with the semicircle itself. Bode plots were also obtained as a function of current density, as shown in Fig. 5(b) where two major features can be seen in the form a phase shift. A peak in the phase shift indicates an increase of the imaginary impedance, indicative for a capacitive effect. At low current densities, a large peak is present below 1 Hz, and a minimum in the phase shift can be seen around 100 Hz. As the current density is

increased, the peak below 1 Hz decreases significantly, while a subtle peak emerges between 10 and 500 Hz, shown in the inset of Fig. 5(b). In addition, another increase of the phase shift is visible at frequencies above 1000 Hz; however, this increase is independent of the applied current. Furthermore, it is a high frequency dispersion or stray capacitance of the reference electrodes, which is caused by the limited exchange capacity of the glass frit at high frequencies and appears as a capacitance effect in the Bode plot. Additionally, 1 M  $\text{Na}_2\text{SO}_4$  vs.  $\text{Na}_2\text{SO}_4$  was tested, similar to the case of the co-ions does this electrolyte combination also contain co-ions at the membrane–membrane interface and showed similar behavior as for 1 M  $\text{KHCO}_3$  vs. KOH (see Fig. S5†).

EIS experiments were also performed at different current densities in the no co-ions<sub>mem</sub> case ( $\text{H}_2\text{SO}_4$  vs. KOH) and reveal a completely different behavior compared to the prior case. Nyquist plots similarly show a changing origin of the semicircle, but no variation in the radius of the semicircle with increasing current density, shown in Fig. 6(a). The Bode plot shows no peak in phase shift below 1 Hz and only a peak between 10 and 1000 Hz is observed, which does not change significantly with different current densities, as shown in Fig. 6(b). At higher frequencies, a stray capacitance is visible, similar to the case with no co-ions<sub>mem</sub>.

When the data from Fig. 5 and 6 is compared, the previously described equivalent circuit can be matched to specific frequency ranges and physical phenomena. The first component of the equivalent circuit, related to the ohmic resistance ( $R_\Omega$ ), depends primarily on the conductivity of the membrane, relating to the mobility of ions in the membrane layers as shown schematically in Fig. 7(a). It is important to note that EIS does not allow the ability to determine  $R_\Omega$  without including the conductivity of the electrolyte, which should be limited due to the relatively short distance between the reference electrodes and the membrane. The second component of the equivalent circuit is related to the water dissociation reaction, shown schematically in Fig. 7(b). Based on the presence of two peaks in the co-ions case (1 M  $\text{KHCO}_3$  vs. KOH), and only one peak in the no co-ion case (1 M  $\text{H}_2\text{SO}_4$  vs. KOH), it is likely that the shared peak in the frequency range between 10 and 1000 Hz (for this

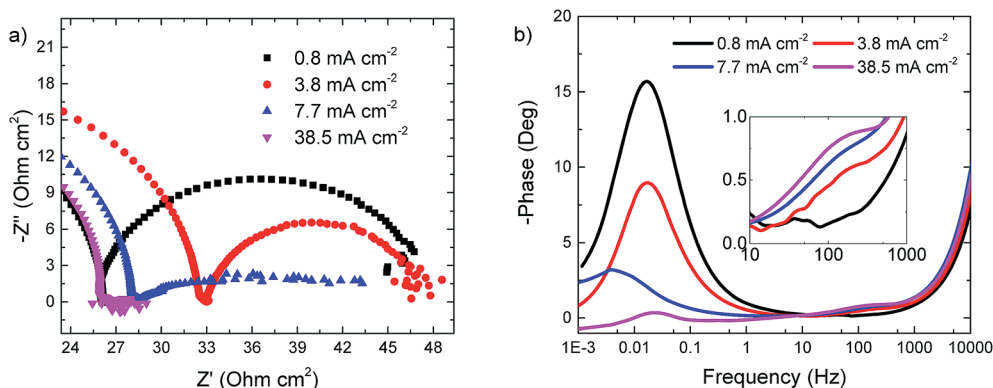


Fig. 5 Presence of co-ions (1 M  $\text{KHCO}_3$  vs. KOH) in function of DC current with an amplitude of 50% of the direct current. (a) Nyquist plot and (b) Bode plot with varying frequency.

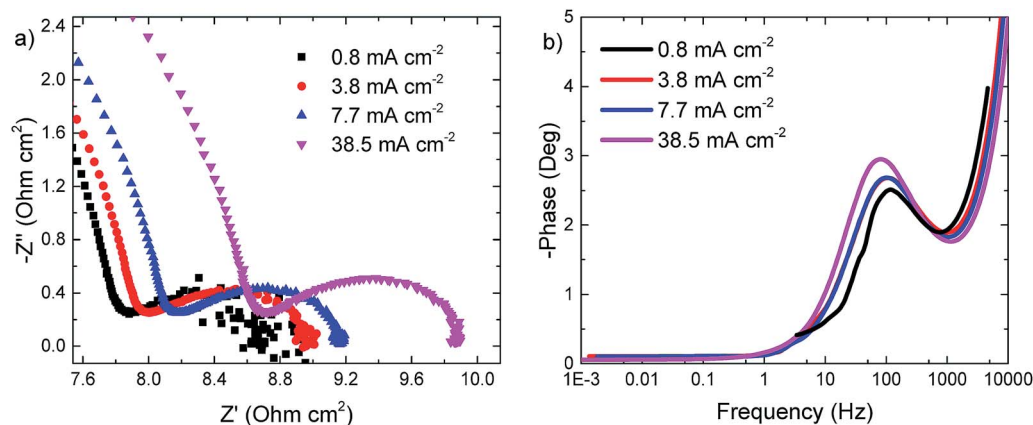


Fig. 6 Impedance results of the no co-ions<sub>mem</sub> case (1 M H<sub>2</sub>SO<sub>4</sub> vs. KOH) in function of DC current with an amplitude of 50% of the direct current. (a) Nyquist plot and (b) Bode plot with varying frequency.

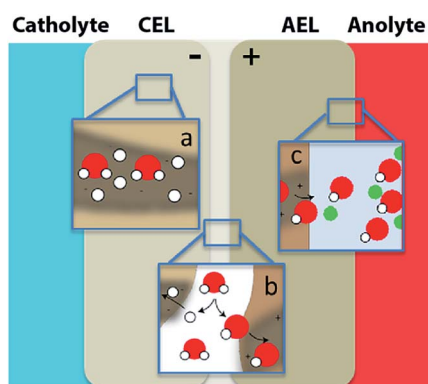


Fig. 7 Schematic representation of (a) ohmic losses, (b) water dissociation reaction, and (c) diffusion boundary layer.

specific membrane) is related to the water dissociation reaction that occurs in both cases above  $j_{\text{plateau}}$ . This peak is represented in the equivalent circuit with a resistor ( $R_{\text{WDR}}$ ) and a constant phase element ( $Q_{\text{DL}}$ ) in parallel. The peaks are fitted with ZView2, and an example of the fitting curve is given in Fig. S4.† For the no co-ions<sub>mem</sub> case, Table 1 shows the fitted  $R$  and  $Q$  values, alongside the position of the phase shift peaks. The slight variation in the fitted values corresponds with the limited change in the kinetics of the WDR that may be related to ageing

Table 1 Impedance data of the no co-ion case (1 M H<sub>2</sub>SO<sub>4</sub>–KOH), with the WDR semicircle fitted *via* an equivalent circuit.  $f_{\text{WDR}}$  is the frequency at which the phase shift ( $\theta_{\text{WDR}}$ ) is maximised.  $R_{\text{WDR}}$ ,  $Q_{\text{DL}}$  and  $n_{\text{WDR}}$  are resistance, constant phase element and fitting parameter of the WDR semicircle

$j$ , mA cm <sup>-2</sup>	$-\theta_{\text{WDR}}$ , Deg	$f_{\text{WDR}}$ , Hz	$R_{\text{WDR}}$ , Ω cm <sup>2</sup>	$Q_{\text{DL}}$ , mF cm <sup>2</sup>	$n_{\text{WDR}}$ , —
0.8	2.51	116.5	0.91	7.80	0.85
3.8	2.68	107.8	1.07	6.50	0.85
7.7	2.69	100.0	1.08	7.15	0.85
38.5	2.95	79.6	1.29	7.41	0.85

of the BPM, as will be discussed later. In the case of H<sub>2</sub>SO<sub>4</sub> vs. KOH, the local environment at the catalytic active sites remains similar since the bulk electrolyte contains the same mobile species at these different currents, consisting mostly of fixed charges, water and protons or hydroxide ions, depending on the membrane layer. The role of the flux of ions produced at the membrane–membrane interface does not affect the WDR peak, since the flux has to match the consumption of ions at the electrode. The amount of crossover of co-ions at 50 mA cm<sup>-2</sup> is 1.5% (see Table S1†), while the rest of the current transported towards the electrodes comes from the WDR.

Tables 2 and 3 show the fitted RC-values for the co-ions case (1 M KHCO<sub>3</sub> vs. KOH) for the WDR and DBL peak, respectively. In this case, both peaks are dependent on the applied current. The lower  $n$ -value of the WDR capacitor indicates that the capacitor is less ideal than the no co-ions<sub>mem</sub> case. Furthermore, when a current is applied below the plateau current density,  $j_{\text{plateau}}$ , *e.g.* in the case of 0.8 mA cm<sup>-2</sup>, no WDR peak is visible. Indeed, analysis from an ion-coupled plasma optical emission spectrometer (ICP-OES) showed a 100% co-ion crossover (see Table S2†), implying that below  $j_{\text{plateau}}$  no net WDR occurs. At higher currents, a lower capacitance in the electrical double layer is observed, trending towards similar values as in the case with no co-ions<sub>mem</sub>. In addition, the resistance of the WDR converges towards similar values for both electrolyte pairs as the current densities increases, indicating that the conditions near

Table 2 Impedance data of the co-ion case (1 M KHCO<sub>3</sub>–KOH), with WDR semicircle fitted *via* an equivalent circuit.  $f_{\text{WDR}}$  is the frequency at which the phase shift ( $\theta_{\text{WDR}}$ ) is maximised.  $R_{\text{WDR}}$ ,  $Q_{\text{DL}}$  and  $n_{\text{WDR}}$  are resistance, constant phase element and fitting parameter of the WDR semicircle

$j$ , mA cm <sup>-2</sup>	$-\theta_{\text{WDR}}$ , Deg	$f_{\text{WDR}}$ , Hz	$R_{\text{WDR}}$ , Ω cm <sup>2</sup>	$Q_{\text{DL}}$ , mF cm <sup>2</sup>	$n_{\text{WDR}}$ , —
0.8	—	—	—	—	—
3.8	0.55	146.8	1.95	3.64	0.60
7.7	0.64	108.0	1.69	6.50	0.60
38.5	0.80	125.9	1.30	9.10	0.70

**Table 3** Impedance data of the co-ions case (1 M  $\text{KHCO}_3$  vs. KOH), with DBL semicircle fitted via equivalent circuit.  $f_{\text{DBL}}$  is the frequency at which the phase shift ( $\theta_{\text{DBL}}$ ) is maximised.  $R_{\text{DBL}}$ ,  $Q_{\text{DBL}}$  and  $n_{\text{DBL}}$  are resistance, constant phase element and fitting parameter of the DBL semicircle

$j$ , $\text{mA cm}^{-2}$	$-\theta_{\text{DBL}}$ , Deg	$f_{\text{DBL}}$ , Hz	$R_{\text{DBL}}$ , $\Omega \text{ cm}^2$	$Q_{\text{DBL}}$ , $\text{F cm}^2$	$n_{\text{DBL}}$ , —
0.8	15.68	0.017	22.35	0.91	0.95
3.8	8.97	0.017	13.00	1.39	1.00
7.7	3.19	0.004	—	—	—
38.5	0.34	0.025	0.52	~19.5	0.70

the membrane–membrane interface are the same at those conditions. At these higher currents, fewer co-ions—in this case  $\text{K}^+$ —are present at the interface, which corresponds more to the situation of the case of no co-ions<sub>mem</sub>. The increase in  $R_{\text{WDR}}$  compared to the no co-ions<sub>mem</sub> case is clarified via Fig. 8, which shows the  $i$ - $V$  curve (red) of a BPM in the co-ion case (1 M  $\text{KHCO}_3$  vs. KOH). In this figure, a plateau current density is observed between 0.4 and 0.8 V of the BPM potential.

The third component of the equivalent circuit is related to the diffusion boundary layer at the electrolyte–membrane interface, and is only visible at frequencies below 1 Hz, as shown in Fig. 5 experimentally and Fig. 7(c) schematically. The EIS data obtained from the fitted DBL semicircle for the co-ion case is shown in Table 3. Quantifying the resistance is useful to determine the energy loss of this component as it is noticeable during direct current operation, whereas the  $Q_{\text{DBL}}$  is not noticeable during direct current operations. However,  $Q_{\text{DBL}}$  is still a good measure for the build-up of charge caused by the change of transport numbers of the ions that move across in the membrane layer compared to the bulk solution.<sup>23</sup> At lower current densities, diffusion and migration are of the same order of magnitude, indicating that ion transport is not dominated by either of them, and co-ions with their respective charge are present at the interfaces. As a result of the presence of these co-ions, a lower capacitance is noticed at lower current densities (see Table 2).

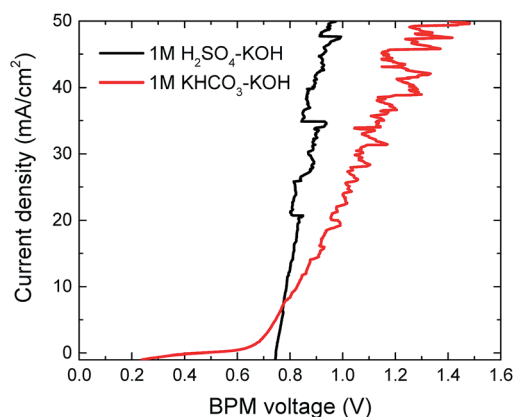


**Fig. 8**  $i$ - $V$  curves of a BPM for the co-ion case (1 M  $\text{KHCO}_3$  vs. KOH) in red and for the no-co-ion case (1 M  $\text{H}_2\text{SO}_4$  vs. KOH) in black. Both curves are obtained with a galvanodynamic scan at a scan rate  $-0.1 \text{ mA cm}^{-2} \text{ s}^{-1}$  with the flow cell.

Both for the WDR and the DBL peak, the decrease in the capacitance at higher current densities for the co-ions case (1 M  $\text{KHCO}_3$  vs. KOH) can possibly be explained by changes in concentrations of species at the respective interfaces. One hypothesis to explain this is that the supporting electrolyte is more conducting at higher current densities, as  $\text{H}^+$  and  $\text{OH}^-$  are the most mobile ions. In addition, the buffer capacity of the electrolyte near the BPM may decrease due to the change in local pH, as simulated by Ke *et al.*<sup>20</sup> This decrease in buffer capacity results in a lower capacitance since the charge can no longer be stored near the BPM.<sup>41</sup> At higher current densities, there will be relatively less transport of co-ions at steady state because of the direction of the migration component, which transports the co-ions away from the BPM. Combined with the change of local pH, this reduces the difference in transport numbers of the ions ( $\text{H}^+$  and  $\text{OH}^-$  for these high currents) that are transported in the membrane layer compared to the bulk solution. In the no co-ions<sub>mem</sub> case (1 M  $\text{H}_2\text{SO}_4$  vs. KOH), this difference in transport number at the membrane–electrolyte interface is rather small, since the concentration of protons is similar to the concentration in the bulk solution. Similar trends are observed when negative currents are applied for the case of no co-ions<sub>mem</sub> ( $\text{H}_2\text{SO}_4$  vs. KOH), while a plateau also appears in the  $i$ - $V$  curve around  $-35 \text{ mA cm}^{-2}$  along with a DBL component in the Bode plot (see Fig. S1†). Although this mechanism is not yet fully understood, it does imply that the equivalent circuit shown in Fig. 1(d) is generalizable for different combinations of pHs surrounding the BPM, as well as different concentrations that will be discussed in the following section.

### Concentration effect

In order to understand the effect of the concentrations of ions in and around the BPM, EIS data were obtained for electrolyte pairs as a function of electrolyte concentration. When the concentration of  $\text{H}_2\text{SO}_4$ -KOH was lowered from 1 M to 0.1 M, for the no co-ions<sub>mem</sub> case, the WDR peak is reduced in size, as shown in Fig. 9 and Table S3† with the fitted results. However, no WDR peak is visible for 0.1 M  $\text{KHCO}_3$  vs. KOH, as the peak might be hidden within the stray capacitance.

From the  $i$ - $V$  curve of the 0.1 M  $\text{H}_2\text{SO}_4$ /KOH case (Fig. S3†), the kinetics of the WDR seems to be lowered compared to the higher concentration case. Also, the WDR capacitance has reduced (Table S3†), indicating that fewer mobile charge species are present in the membrane–membrane interface. This is schematically shown in Fig. 10, with the concentrations profile of three electrolytes with a concentration of 0.1 M when a current is applied to the system. The flux of ions will create a DBL at the membrane–solution interface, which is smaller than in the case of a 1 M concentration (Fig. 3). Since there is a lower concentration of co-ions in the bulk, the concentration gradient is also lower, reducing the driving force for ions with a similar layer charge as the fixed charges to diffuse into the membrane layer. Because of electroneutrality, this then leads to a lower concentration of the ions of opposing charge, which reduces the charge at the membrane–membrane interface.

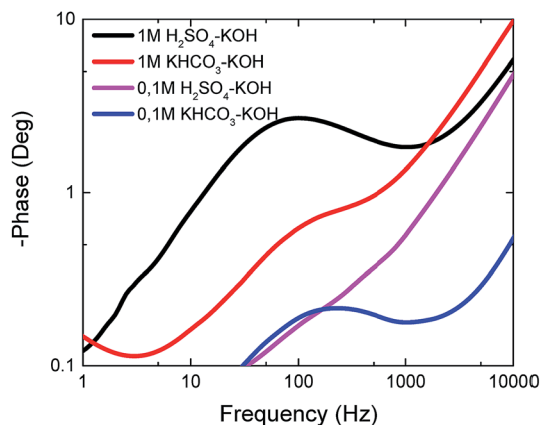


Fig. 9 Bode plot of 1 M and 0.1 M electrolyte concentrations across the BPM. Curves were obtained at  $7.7 \text{ mA cm}^{-2}$  with 50% amplitude.

### Ageing of BPM

In this section, we introduce electrochemical impedance spectroscopy as a tool to *in situ* observe the ageing of a BPM and membranes in general. When a BPM is used in industrial applications, high activity and durability are of high importance. The performance of the BPM should also be measurable in operation, which is possible by applying a small perturbation to the DC current or voltage, resulting in the typical EIS graphs presented above. Differentiating between the individual components, such as conductivity of the membrane or kinetics of the WDR, reveals which methods can be used to prolong the lifetime of the membrane, *e.g.* lowering the current or replacing the electrolyte(s), or, if that is no longer sufficient, renewing the BPM.

For this purpose, a BPM was tested in a flow cell (see Fig. S2†) of  $10 \text{ cm}^2$  with a flow rate of  $0.07 \text{ cm}^3 \text{ s}^{-1}$  in  $1 \text{ M H}_2\text{SO}_4$  vs.  $1.3 \text{ M KOH}$ . An impedance measurement was performed at the beginning of the experiment with an applied direct current of  $20 \text{ mA cm}^{-2}$  and an EIS amplitude of  $5 \text{ mA cm}^{-2}$ . After this, for 5 days a DC current of 0, 50, and  $100 \text{ mA cm}^{-2}$  was applied, respectively. Immediately after this experiment, the same EIS measurement was repeated. Similarly, 0 and  $50 \text{ mA cm}^{-2}$  were tested for  $1 \text{ M KHCO}_3$  vs.  $\text{NaOH}$ . Both experiments for all current densities are shown in Fig. 11, and its parameters are described in Table 4.

For the experiment with no current applied, only a slow exchange of co-ions *via* diffusion was observed, driven by the concentration gradient across the BPM. For the no co-ions<sub>mem</sub> case ( $\text{H}_2\text{SO}_4$  vs.  $\text{KOH}$ ), analysis from ICP-OES showed an exchange of 10%  $\text{K}^+$  from the anolyte towards the catholyte after 5 days of open-circuit operation. Once a current was applied, the crossover increased to 20% and 32% for 50 and  $100 \text{ mA cm}^{-2}$ , which was 11% and 13.5% of the applied current, respectively. The crossover of  $\text{SO}_4^{2-}$  was minor compared to  $\text{K}^+$ , as can be seen in Table S1.† The increase of the crossover can be described by the extra migration component that is related to the electric field gradient on the system, which transports  $\text{K}^+$  through the membrane towards the cathode that attracts positive charged ions. These high crossover numbers indicate that this membrane is not ideal for systems that are sensitive to fouling from neighboring co-ions. This strong degradation is not visible in the co-ions case (Fig. 11(b)). Alongside the strong degradation of the membrane in extreme conditions, there is a strong need for further membrane development using the discussed techniques in order to successfully implement BPMs in current technologies and reduced energy costs.

When the system is subject to an applied current density of  $50 \text{ mA cm}^{-2}$  for 5 days, the increase in the potential over the BPM is around 170 mV. EIS results (Fig. 11(a), two measurements in red), show the individual increases of the membrane components can be determined. The ohmic resistance increased from  $3.2 \Omega \text{ cm}^2$  to  $4.2 \Omega \text{ cm}^2$ , which corresponds to a voltage loss of 50 mV. This extra ohmic resistance loss is associated to the bulk of the membrane layers, which is known from literature to occur *via* charge leaching at high pH.<sup>42</sup> The difference in the width of the two semicircles resulted in another 50 mV increase. The remaining extra potential of the 170 mV can be attributed to the finite membrane selectivity, which causes ion crossover, lowering the conductivity and resulting in an extra ohmic loss. Other effects have a minimal impact on the ageing including the diffusion boundary component, which is neglected since this component is negligible for the no co-ions<sub>mem</sub> case ( $\text{H}_2\text{SO}_4$  vs.  $\text{KOH}$ ), and the pH remained nearly constant throughout the experiment.

The increase in the WDR resistance after ageing is noteworthy, especially since it is not accompanied by an increase in

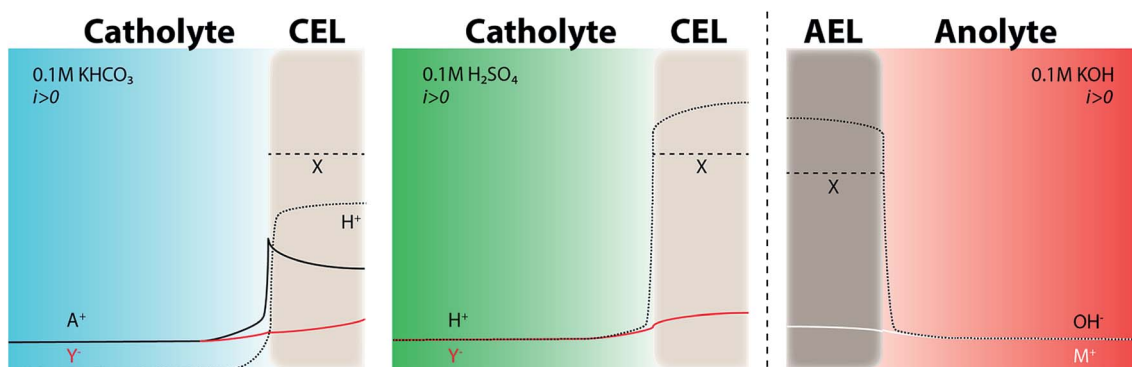


Fig. 10 Qualitative estimation of concentration profiles for diluted salt concentrations in the electrolyte.

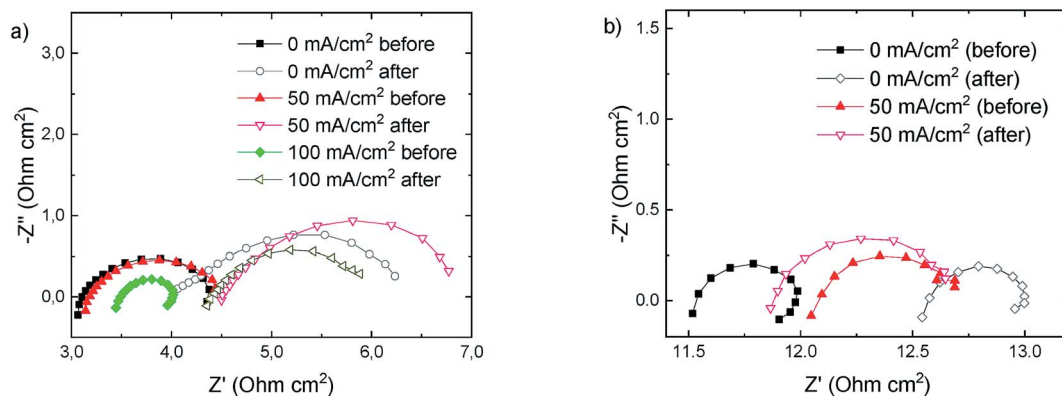


Fig. 11 Ageing of a BPM over 5 days (a) at 0, 50 and 100 mA cm<sup>-2</sup> in 1 M H<sub>2</sub>SO<sub>4</sub> and 1.3 M KOH and (b) at 0 and 50 mA cm<sup>-2</sup> in 1 M KHCO<sub>3</sub> and 1 M NaOH in a flow cell with 60 rpm. EIS performed with a frequency range between 10 kHz and 0.4 Hz. Lower frequencies are not shown because of the noise limitations of the flow cell (e.g., due to gas bubbles) in that frequency range.

Table 4 Impedance data of WDR semicircles after stability measurements

Electrolyte	Current density, mA cm <sup>-2</sup>	State	$R_{\text{WDR}}$ , $\Omega$ cm <sup>2</sup>	$Q_{\text{WDR}}$ , F cm <sup>2</sup>	$n_{\text{WDR}}$ , —
1 M H <sub>2</sub> SO <sub>4</sub> -KOH	0	Before	1.30	0.35	0.80
	0	After	2.10	0.30	0.80
	50	Before	1.30	0.55	0.75
	50	After	2.40	0.26	0.85
	100	Before	0.52	0.25	0.90
	100	After	1.70	0.52	0.75
1 M KHCO <sub>3</sub> -NaOH	0	Before	0.50	0.40	0.85
	0	After	0.45	0.55	0.85
	50	Before	0.60	0.55	0.85
	50	After	0.85	0.55	0.85

the capacitive component in the equivalent circuit. The capacitor is represented as a double layer in the internal interface because of the strong polarized environment. There are two possible explanations for the decrease in the kinetics. The first is the reduced activity of the catalyst at the interface, which performs reactions (1) and (2), due to lowered number of fixed charges *via* recombination—where positive and negative fixed charges recombine to form a neutral component. The importance of the catalyst loading has been studied earlier in relation with required voltage, and in general the lower the catalyst loading, the higher voltage is required.<sup>11,39</sup> The second explanation is the widened interface thickness, which was proven in literature to have an important impact on the voltage.<sup>15</sup> Here, the integration of the layers at the membrane–membrane interface separated in time. Therefore, the interfacial catalyst and the electronic properties of the interface itself should be main focus points in the future developments and minimization of operational losses in BPMs.

## Conclusions

In this work, a bipolar membrane was examined using electrochemical impedance spectroscopy, which makes it possible to differentiate electronic information among the different

components of the membrane. In particular, the interface between the two membrane layers was of interest. At this interface, the water dissociation reaction occurs, which dissociates water into protons and hydroxide ions under an applied potential. However, depending on the electrolyte(s) surrounding the membrane, the *i*-*V* curves behaves differently. Therefore, two cases were studied, one without co-ions and the other with co-ions. It was demonstrated that the individual components, such as the kinetics of the water dissociation reaction and the capacitance of the diffusion boundary layer, can be identified using EIS, contributing to understanding of electrochemical elements within the BPM. EIS shows that at low current densities below the plateau current density, a different behavior exists, which is dominated by co-ion transport. The co-ions case showed a plateau at a low current density, where co-ions seem to be responsible for the charge transport (shown with ICP-OES analysis) and no WDR peak is visible in the impedance measurement. At higher current densities for KHCO<sub>3</sub>/KOH, and at all (positive) current densities for the H<sub>2</sub>SO<sub>4</sub>/KOH case, impedance spectra show a clear capacitive element that is ascribed to the WDR. Finally, EIS has proven to be a useful tool to monitor the ageing of a BPM and to determine which component is affected most by the ageing, which is important to design and implement BPMs in electrochemical cells for industrial applications.

## Conflicts of interest

There are no conflicts to declare.

## Acknowledgements

This research received funding from the Netherlands Organisation for Scientific Research (NWO) under project number 733.000.008 in the framework of the Solar to Products programme co-funded by Shell Global Solutions International. The authors would like to thank Baukje Terpstra for the ICP-OES measurements, Dr Thomas Burdyny for fruitful discussions and Anirudh Venugopal for helping during experiments.

## References

- 1 IPCC, Global Warming of 1.5 °C. An IPCC Special Report on the impacts of global warming of 1.5 °C above pre-industrial levels and related global greenhouse gas emission pathways, in *the context of strengthening the global response to the threat of climate change*, 2018.
- 2 FCH JU, *Development of Water Electrolysis in the European Union*, 2014.
- 3 T. Burdyny and W. A. Smith, *Energy Environ. Sci.*, 2019, **12**, 1442–1453.
- 4 M. Jouny, W. Luc and F. Jiao, *Ind. Eng. Chem. Res.*, 2018, **57**, 2165–2177.
- 5 S. Ma, R. Luo, S. Moniri, Y. Lan and P. J. A. Kenis, *J. Electrochem. Soc.*, 2014, **161**, F1124–F1131.
- 6 J. Luo, D. A. Vermaas, D. Bi, A. Hagfeldt, W. A. Smith and M. Grätzel, *Adv. Energy Mater.*, 2016, **6**, 1–7.
- 7 Y. C. Li, D. Zhou, Z. Yan, R. H. Gonçalves, D. A. Salvatore, C. P. Berlinguette and T. E. Mallouk, *ACS Energy Lett.*, 2016, **1**, 1149–1153.
- 8 D. A. Salvatore, D. M. Weekes, J. He, K. E. Dettelbach, Y. C. Li, T. E. Mallouk and C. P. Berlinguette, *ACS Energy Lett.*, 2017, 149–154.
- 9 D. A. Vermaas and W. A. Smith, *ACS Energy Lett.*, 2016, **1**, 1143–1148.
- 10 N. M. Vargas-Barbosa, G. M. Geise, M. A. Hickner and T. E. Mallouk, *ChemSusChem*, 2014, **7**, 3017–3020.
- 11 M. B. McDonald, S. Ardo, N. S. Lewis and M. S. Freund, *ChemSusChem*, 2014, **7**, 3021–3027.
- 12 H. Strathmann, J. J. Krol, H. J. Rapp and G. Eigenberger, *J. Membr. Sci.*, 1997, **125**, 123–142.
- 13 D. A. Vermaas, S. Wiegman, T. Nagaki and W. A. Smith, *Sustainable Energy Fuels*, 2018, **2**, 2006–2015.
- 14 J. Balster, S. Srinantharajah, R. Sumbharaju, I. Pünt, R. G. H. Lammertink, D. F. Stamatialis and M. Wessling, *J. Membr. Sci.*, 2010, **365**, 389–398.
- 15 C. Shen, R. Wycisk and P. N. Pintauro, *Energy Environ. Sci.*, 2017, **10**, 1435–1442.
- 16 J. Pan, L. Hou, Q. Wang, Y. He, L. Wu, A. N. Mondal and T. Xu, *Mater. Chem. Phys.*, 2017, **186**, 484–491.
- 17 A. J. Bard and L. R. Faulkner, *Electrochemical Methods Fundamentals and Applications*, Wiley, 1994.
- 18 R. El Moussaoui, G. Pourcelly, M. Maeck, H. D. Hurwitz and C. Gavach, *J. Membr. Sci.*, 1994, **90**, 283–292.
- 19 H. W. Rösler, F. Maletzki and E. Staude, *J. Membr. Sci.*, 1992, **72**, 171–179.
- 20 K. Sun, R. Liu, Y. Chen, E. Verlage, N. S. Lewis and C. Xiang, *Adv. Energy Mater.*, 2016, **6**, 1–7.
- 21 F. G. Wilhelm, N. F. A. Van Der Vegt, H. Strathmann and M. Wessling, *J. Appl. Electrochem.*, 2002, **32**, 455–465.
- 22 H. Holdik, A. Alcaraz and S. Mafe, *J. Electroanal. Chem.*, 1998, **442**, 13–18.
- 23 P. Długołęcki, P. Ogonowski, S. J. Metz, M. Saakes, K. Nijmeijer and M. Wessling, *J. Membr. Sci.*, 2010, **349**, 369–379.
- 24 V. Zabolotskii, N. Sheldeshov and S. Melnikov, *Desalination*, 2014, **342**, 183–203.
- 25 S. Mafe, A. Alcaraz, H. Holdik, T. Ruf and P. Ramo, *J. Membr. Sci.*, 1998, **150**, 43–56.
- 26 A. Alcaraz, P. Ramirez, J. A. Manzanares and S. Mafe, *J. Phys. Chem. B*, 2001, **105**, 11669–11677.
- 27 H. D. Hurwitz and R. Dibiani, *J. Membr. Sci.*, 2004, **228**, 17–43.
- 28 M. S. Park, W. Joo and J. K. Kim, *Langmuir*, 2006, **22**, 4594–4598.
- 29 P. Ramirez, J. A. Manzanares and S. Mafe, *Berichte der Bunsengesellschaft für physikalische Chemie*, 1991, **95**, 499–503.
- 30 M. Wien, *Ann. Phys.*, 1924, **3**, 161–181.
- 31 R. Simons, *Nature*, 1979, **280**, 824–826.
- 32 R. Simons, *Electrochim. Acta*, 1985, **30**, 275–282.
- 33 R. Simons and G. Khanarian, *J. Membr. Biol.*, 1978, **38**, 11–30.
- 34 A. H. Galama, J. W. Post, M. A. Cohen Stuart and P. M. Biesheuvel, *J. Membr. Sci.*, 2013, **442**, 131–139.
- 35 F. G. Donnan, *Electrochemistry*, 1911, **17**, 572.
- 36 P. Sizat and G. Pourcelly, *J. Membr. Sci.*, 1997, **123**, 121–131.
- 37 J. Bisquert, G. Garcia-Belmonte, F. Fabregat-Santiago and P. R. Bueno, *J. Electroanal. Chem.*, 1999, **475**, 152–163.
- 38 A. Alcaraz, P. Ramirez, S. Mafe and H. Holdik, *J. Phys. Chem.*, 1996, **3654**, 15555–15561.
- 39 Z. Yan, L. Zhu, Y. C. Li, R. J. Wycisk, P. N. Pintauro, M. A. Hickner and T. E. Mallouk, *Energy Environ. Sci.*, 2018, **11**, 2235–2245.
- 40 A. Wuttig, Y. Yoon, J. Ryu and Y. Surendranath, *J. Am. Chem. Soc.*, 2017, **139**, 17109–17113.
- 41 R. E. G. Van Hal, J. C. T. Eijkel and P. Bergveld, *Sens. Actuators, B*, 1995, **25**, 201–205.
- 42 J. R. Varcoe, P. Atanassov, D. R. Dekel, A. M. Herring, M. A. Hickner, P. A. Kohl, A. R. Kucernak, W. E. Mustain, K. Nijmeijer, K. Scott and L. Zhuang, *Energy Environ. Sci.*, 2014, **7**, 3135–3191.